Ibn Al-Haitham Journal for Pure and Applied Sciences
Journal homepage: jih.uobaghdad.edu.iq
PISSN: 1609-4042, EISSN: 2521-3407
IHJPAS. 2026; 39(2)

Direct Reaction Model Study of Radiative Proton Capture in Light Nuclei Relevant to ^{9}B, ^{7}Li, and ^{7}Be

Ali H. Hammadi[1*], and Ali A. Alzubadi[2]
[1,2]Department of Physics, College of Science, University of Baghdad, Baghdad, Iraq
*Corresponding Author

Received: 22/June /2025
Accepted: 14/January/2026
Published: 20/April/2026
doi.org/10.30526/39.2.4234

Abstract

This study investigates radiative proton capture reactions in light nuclei such as [^{9}B- ^{7}Li, - ^{7}Be], which are crucial in stellar nucleosynthesis and energy production. The Woods-Saxon potential model was employed to describe nuclear interactions, and the Schrödinger equation was solved to determine bound and continuum state wave functions accurately. Astrophysical S-factors and reaction cross-sections were calculated at low energies characteristic of stellar environments, accounting for nuclear resonance effects that significantly enhance reaction probabilities. Radiative proton capture reactions, of the form A(p,γ)B, are fundamental processes in nuclear astrophysics. They are the primary mechanism for synthesizing elements in both hydrostatic and explosive stellar environments. he formation of ^{7}Li and ^{7}Be is a key outcome of the Big Bang. The reaction ^{3}He(α,γ)^{7}Be is the primary source of ^{7}Be, which later decays to ^{7}Li. Understanding the ^{7}Be system is thus crucial for predicting the primordial lithium abundance. The theoretical results show strong agreement with experimental data, validating the model's reliability. These findings provide precise inputs for refining nuclear reaction rates in stellar evolution models, thereby improving predictions of elemental synthesis and energy generation in stars.

Keywords: Radiative capture, Woods-Saxon Potential, Astrophysical S-Factor, Direct Reaction, Phase Shift.

1. Introduction

Nuclear astrophysics investigates some of the most intriguing inquiries in the natural world what are the sources of the elements that are indispensable for life. What is the estimated age of the universe, what is the process by which the Sun, its companion, the stars, along our Galaxy, was formed and developed we have acquired a fundamental, albeit incomplete, comprehension of the processes that regulate the development of stars and contribute to the synthesis of elements [1]. Radiative capture reactions are a fundamental process in astrophysics, where a proton or neutron interacts with a nucleus to form a new nucleus, accompanied by the emission of electromagnetic radiation. These processes play a crucial role in element formation within stars and other astrophysical phenomena [2]. Radiative capture reactions are broadly classified into neutron capture and proton capture. Neutron capture dominates the slow (s-) and rapid (r-) synthesis of heavier elements [3]. Proton capture reactions are central to hydrogen-burning cycles, particularly the carbon-nitrogen-oxygen (CNO) chain, which governs energy generation in stars more massive than the Sun [4,5].The p-p process (proton capture) creates uncommon, proton-rich isotopes. Supernovae's high-temperature conditions entail adding protons to nuclei to overcome electrostatic repulsion to produce isotopes of elements like molybdenum and ruthenium, which conventional nucleosynthesis routes cannot make [6,7]. Stars' energy-generating processes—p-p cycle, CNO cycle, HCNO cycle, rp-process [8] etc.—require continual Addition of protons in opposition to the Coulomb barrier. In astrophysical environments such as X-ray bursters. Intense

proton flux at ~several GK and matter density ~of 10^6 g/cm³ causes a fast proton capture process, resulting in a brief thermal burst that peaks in the X-ray [9]. By examining these reactions, we aim to improve the accuracy of reaction rates and astrophysical S-factors (S-F) used in stellar models, while also gaining deeper insight into nuclear structure phenomena such as resonance behavior and level densities near the proton threshold. Moreover, these studies serve as important benchmarks for validating nuclear reaction theories and help provide tighter constraints for astrophysical network calculations. Our ultimate goal is to support a more precise determination of S-F and reaction rates at stellar energies. Insights gained from this work are expected to improve the predictive accuracy of nuclear reaction networks in stellar evolution models and shed further light on the role these reactions play in energy generation and the synthesis of elements within stars [10,11].

2. Materials and Methods

Radiative capture reactions, represented by the formula a+b→c+γ, are fundamental to nuclear /astrophysics. In these reactions, a light projectile (b) is captured by a target nucleus (a), leading to the formation of a compound nucleus (c) and the emission of a gamma-ray photon (γ) to conserve energy and angular momentum [12].

2.1. Bound State Wave Functions and Angular Momentum Coupling

The wave function is defined as:

$$\Psi_{JM}(\vec{r}) = \frac{u_{lj}^{J}(r)}{r}\mathcal{Y}_{\ell j}^{\mathcal{J}\mathcal{M}}(\hat{r}) \quad \textbf{(1)}$$

The term $\Psi_{JM}(\vec{r})$ represents the total wavefunction of the system, characterized by the particular total angular momentum J and its associated projection M,$u_{lj}^{J}(r)$ the radial wave function, and $\mathcal{Y}_{\ell j}^{\mathcal{J}\mathcal{M}}(\hat{r})$ the spin-angular function, which is defined as:

$$\mathcal{Y}_{\mathcal{J}\mathcal{M}}^{\mathcal{J}} = \sum_{m,M_a}\langle jm\, I_a M_a|JM\rangle\ |jm\rangle\,|I_a M_a\rangle, \quad \text{with} \quad |jm\rangle = \sum_{m_l,M_b} Y_{lm_l}(\hat{r})\ \chi_{M_b} \quad \textbf{(2)}$$

Where χ_{M_b} is the spinor wavefunction of particle b and A $\langle jm\, I_a M_a|JM\rangle$ Clebsch-Gordan coefficient is employed here. Radiative capture reactions are modeled within a two-body potential framework, where the interaction between the nuclei of the target and the projectile is described by the Schrödinger equation. For a bound state [13,14]. The radial component of the time-independent Schrödinger equation is expressed as:

$$-\frac{\hbar^2}{2\mu}\left(\frac{d^2}{dr^2} - \frac{l(l+1)}{r^2}\right)u_{lj}(r) + V_{\text{eff}}(r)u_{lj}(r) = Eu_{lj}(r) \quad \textbf{(3)}$$

The effective potential combines central, spin-orbit, and Coulomb interactions:

$$V_{\text{eff}}(r) = V_0(r) + V_{SO}(r) + V_C(r) \quad \textbf{(4)}$$

The central potential is defined by the (WS) form:

$$V_0(r) = -V_0\left[1 + \exp\left(\frac{r-R_0}{a_0}\right)\right]^{-1} \quad \textbf{(5)}$$

and the spin-orbit potential is expressed as:

$$V_{SO}(r) = -V_{SO}\left(\frac{\hbar}{m_\pi c}\right)^2 \frac{1}{r}\frac{d}{dr}\left[1 + \exp\left(\frac{r-R_{SO}}{a_{SO}}\right)\right]^{-1}(\vec{l}\cdot\vec{s}) \quad \textbf{(6)}$$

and the potential for Coulombs is defined as:

$$Vc(r) = \frac{Z_a Z_b e^2}{r} \quad \text{for} \quad r > Rc \quad \textbf{(7)}$$

$$Vc(r) = \frac{Z_a Z_b e^2}{2Rc}\left(3 - \frac{r^2}{R_c^2}\right) \quad \text{for} \quad r < Rc \quad \textbf{(8)}$$

The parameter Zi represents the nucleus' charge number *i* (where *i*=*a*, *b*). RC is the Coulomb radius, typically set equal to R_0. The spin-orbit interaction in Eq. 6 is formulated using the pion Compton wavelength, given as $\frac{\hbar}{m_\pi c}$= 1.414 fm. The parameters V_0, V_{S0}, R_0, a_0, R_{S0}, and a_0 are

carefully adjusted to reproduce the observed ground state energy E_B (or that of an excited state). The radial wavefunction is then normalized according to:

$$\int_0^\infty \left|u_{lj}(r)\right|^2 dr = 1 \quad (9)$$

2.2. Bound and Continuum States

For bound states ($E < 0$), wave functions decay at large r. For continuum states:

$$u^J_{Elj}(r \to \infty) = i\sqrt{\frac{m_{ab}}{2\pi k\hbar^2}}\left[H_l^{(-)}(r) - S_{lJ}H_l^{(+)}(r)\right]e^{i\sigma_l(E)} \quad (10)$$

here, $H_l^{(\pm)}(r)$ are Coulomb wavefunctions is given by:

$$H_l^{(\pm)}(r) = G_l(r) \pm iF_l(r) \quad (11)$$

this expresses the Coulomb wavefunctions $H_l^{(\pm)}(r)$ as combinations of the Coulomb functions of the regular F_l and irregular G_l. σ_l is the Coulomb phase shift, and the scattering matrix is given by $S_{lJ} = e^{2i\delta_{lJ}}$, where δ_{lJ} is the nuclear phase shift. To extract the alteration in phase, the numerical solution is matched to the known asymptotic form at a matching radius R [15] using the logarithmic derivative:

$$\alpha_{lJ} = \left(\frac{du^J_{Elj}/dr}{u^J_{Elj}}\right)_{r=R} \quad (12)$$

This leads to the scattering matrix expressed as:

$$S_{lJ} = \frac{G_l' - iF_l' - \alpha_{lJ}(G_l - iF_l)}{G_l' + iF_l' - \alpha_{lJ}(G_l + iF_l)} \quad (13)$$

A resonance occurs when the phase shift satisfies:

$$\left.\frac{d^2\delta_{lJ}}{dE^2}\right|_{E^R_{lJ}} = 0, \quad \text{and} \quad \left.\frac{d\delta_{lJ}}{dE}\right|_{E^R_{lJ}} > 0 \quad (14)$$

The resonance width is given by:

$$\Gamma^R_{lJ} = 2\left(\left.\frac{d\delta_{lJ}}{dE}\right|_{E^R_{lJ}}\right)^{-1} \quad (15)$$

2.3. Electromagnetic Transitions

Electric multipole transitions dominate radiative capture processes. The transition operator of multipolarity $\lambda\mu$ is [16]:

$$\mathcal{O}_{\mathcal{E}\lambda\mu} = e_\lambda\, r^\lambda Y_{\lambda\mu}(\hat{r}), \quad (16)$$

Where the effective charge e_λ accounts for the centre-of-mass correction [17]:

$$e_\lambda = Z_b e\left(-\frac{m_a}{m_c}\right)^\lambda + Z_a e\left(\frac{m_b}{m_c}\right)^\lambda \quad (17)$$

Where the single-particle radial matrix element [18].Is given by:

$$\left\langle lj \left|\left|r^\lambda Y_\lambda\right|\right| l_0 j_0 \right\rangle = e_\lambda\sqrt{4\pi}\int_0^\infty dr\; r^\lambda\, u^J_{lj}(r)u^{J_0}_{l_0 j_0}(r) \quad (18)$$

2.4. Cross Sections and Astrophysical S-Factor

The cross- section for photo-dissociation is given by:

$$\sigma^{(\lambda)}_\gamma(E_\gamma) = \frac{(2\pi)^3(\lambda+1)}{\lambda[(2\lambda+1)!!]^2}\left(\frac{m_{ab}}{\hbar^2 k}\right)\left(\frac{E_\gamma}{\hbar c}\right)^{2\lambda-1}\frac{dB(\pi\lambda)}{dE} \quad (19)$$

where $E_\gamma = E + |E_B|$, with $|E_B|$ signifies the binding energy of the two-body system comprising particles 'a' and 'b'. For transitions occurring between bound states [19]:

$$\sigma^{(\pi\lambda)}_\gamma(E_\gamma) = \frac{(2\pi)^3(\lambda+1)}{\lambda[(2\lambda+1)!!]^2}\left(\frac{E_\gamma}{\hbar c}\right)^{2\lambda-1} B(\pi\lambda;\, l_0 j_0 J_0 \to ljJ)\delta(E_f - E_i - E_\gamma) \quad (20)$$

where E_i *and* E_f are the energies of the initial and final states. The radiative capture cross section by detailed balance:

$$\sigma^{(rc)}_{(\pi\lambda)}(E) = \left(\frac{E_\gamma}{\hbar c}\right)^{2\lambda-1}\frac{2(2I_c+1)}{(2I_a+1)(2I_b+1)}\sigma^{(\lambda)}_\gamma(E_\gamma) \quad (21)$$

Summing over all allowed transitions and including spectroscopic factors C^2S_i The total capture cross section σ_{nr} [20].is given by:

$$\sigma_{nr}(E) = \sum_{i,\pi,\lambda}(C^2S)_i \ \sigma^{(rc)}_{(\pi\lambda),i}(E) \quad \textbf{(22)}$$

As follows is the definition of the astrophysical S-F for the direct acquisition of charged particles to a continuum state to a bound state [21] :

$$S^{(c)}(E) = E\,\sigma_{nr}(E)\,e^{2\pi\eta(E)}, \quad \text{with} \quad \eta(E) = \frac{Z_a Z_b e^2}{\hbar v} \quad \textbf{(23)}$$

3. Results

The potential parameters in **Table 1**, provide the foundational input for the initial calculations. These include the central and spin-orbit well depths, reduced radius r_o, and diffuseness a_o, which are selected based on conventional values validated in low-energy nuclear reaction studies. Nuclear structure inputs specific to each reaction are compiled in **Table 2**, detailing the ground-state spin-parity configurations, binding energies E_b, potential depths V_b, and spectroscopic factors *SF* for the compound nuclei[22]. These parameters are critical for generating reliable astrophysical S-F and cross-sections and were chosen to reflect both theoretical consistency and agreement with available experimental data[23]. The subsequent sections examine each reaction individually, comparing the calculated observables in experimental results to assess the model's efficacy (**Figures 1-12**).

Table 1. Standard WS potential parameters used in the theoretical modeling of radiative proton capture reactions, including geometric and depth parameters for central and spin-orbit potentials

Parameter	Value	Notes
r_o	1.2 fm	Radius parameter
a_o	0.60 fm	Diffuseness
*V*so	−9.8 MeV	Spin-orbit potential depth
R_O=R_C=R_{S0}	r_o (A+1)$^{1/3}$ fm	Geometric scaling with mass number

Table 2. Nuclear structure parameters for selected (p, γ) reactions

Reaction	J_c	j_0	J_a	E_b (MeV)	V_b	*SF*
^{7}Li(p ,γ)^{8}Be	2^+	$P_{3/2}$	$3/2^-$	17.26	-77.72	1.0
^{7}Be(p, γ)^{8}B	0^+	$p_{3/2}$	$3/2^-$	0.14	-41.22	1.0
^{9}Be(p, γ)^{10}B	3^+	$p_{3/2}$	$3/2^-$	0.2	-6.59	1.0

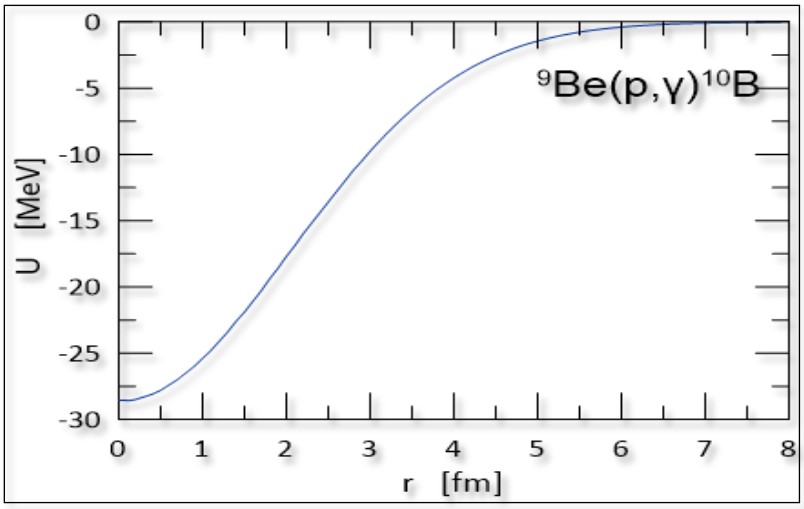

Figure 1. WS potential U(r) for the ^{9}Be(p,γ)^{10}B reaction. Shows the radial dependence of the nuclear interaction.

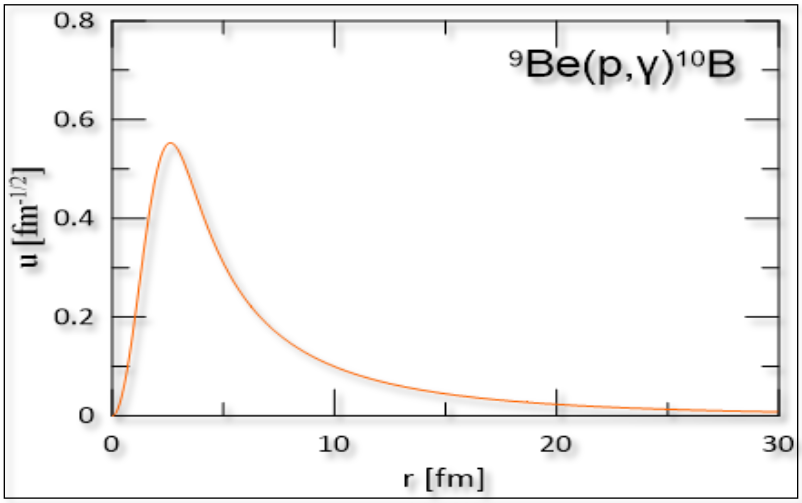

Figure 2. Normalized radial wave function u(r) of the 10B ground state formed in the 9Be(p,γ)10B reaction.

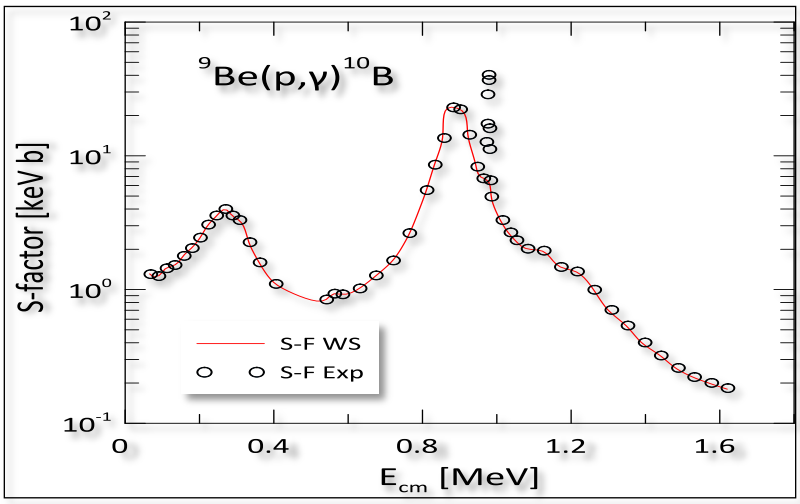

Figure 3. The experimental data points (S-F Exp) represent the measured values. The red curve (S-F) WS corresponds to the theoretical calculations based on the WS model [23].

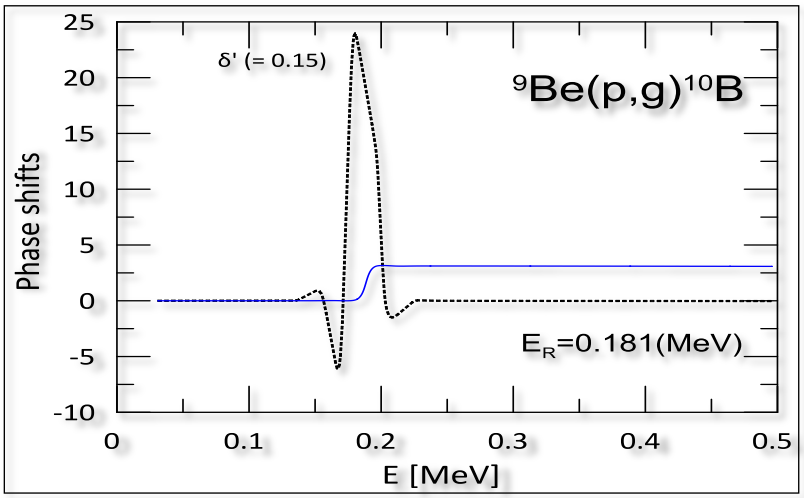

Figure 4. Scattering phase shift (solid line) and its energy derivative (dotted line) for the 9Be(p,γ)10B system showing a resonance at 0.181 MeV.

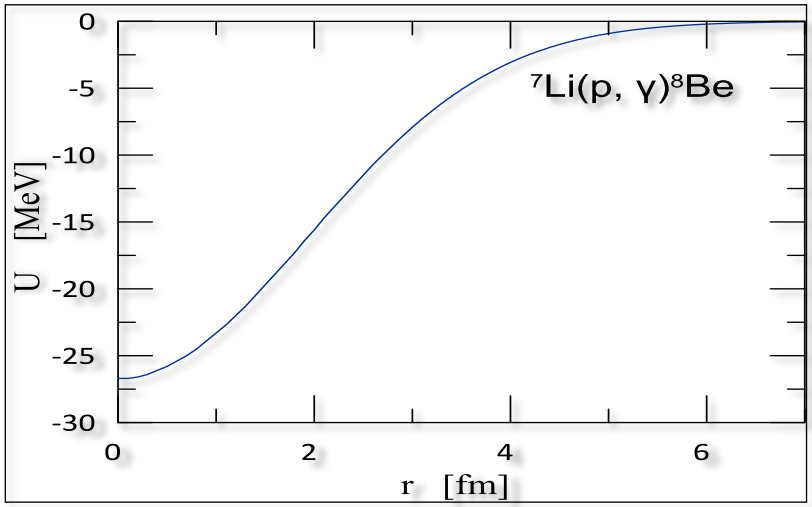

Figure 5. WS potential U(r) for the ^{7}Li(p,γ)^{8}Be reaction. Shows the radial dependence of the nuclear interaction.

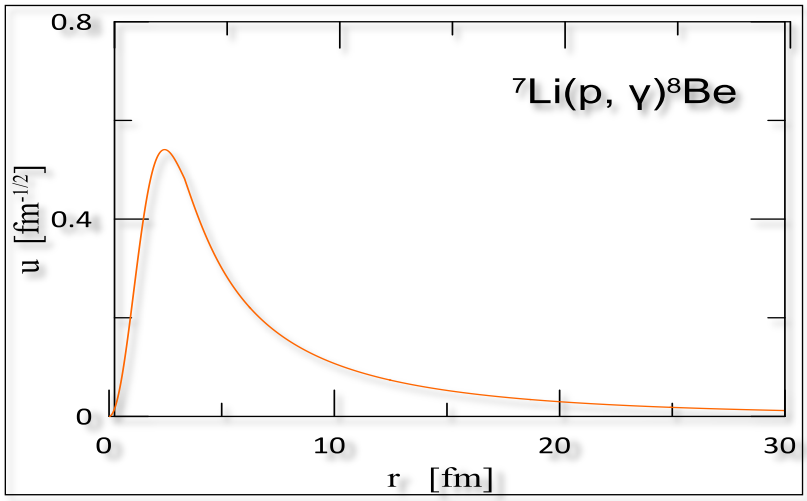

Figure 6. Normalized radial wave function u(r) of the ^{8}Be ground state formed in the ^{7}Li(p,γ)^{8}Be reaction.

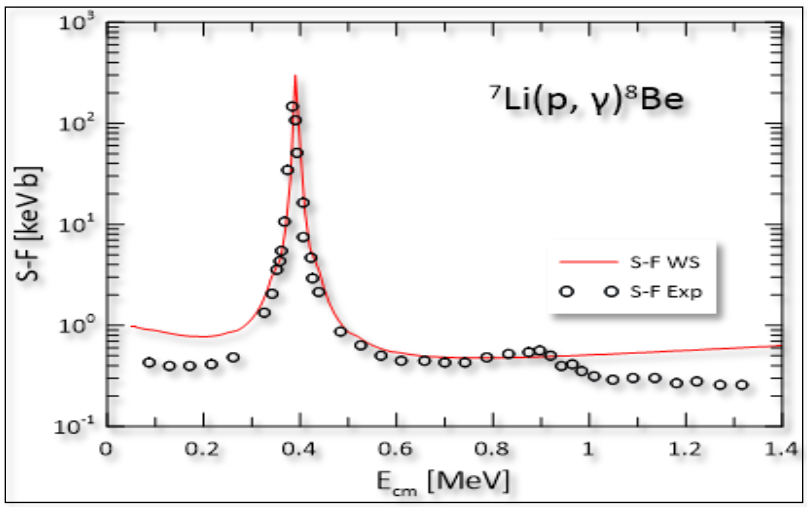

Figure 7. The S-F WS (solid line) represents data derived from a theoretical model, while the S-F Exp (circle) represents results obtained from an experimental procedure [24]

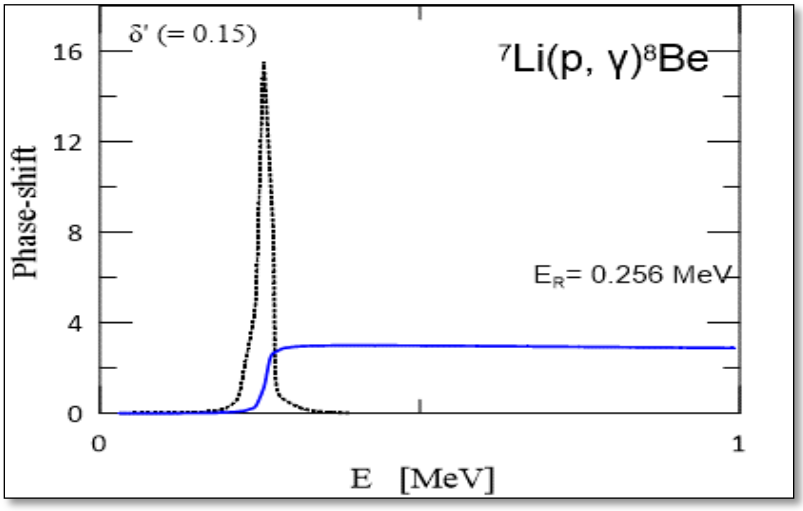

Figure 8. The potential parameters described in the text are used to calculate the phase-shift (solid line) and its derivative (dashed line) for the p+^{7}Li system. The 1+ resonance is detected at 0.256 MeV.

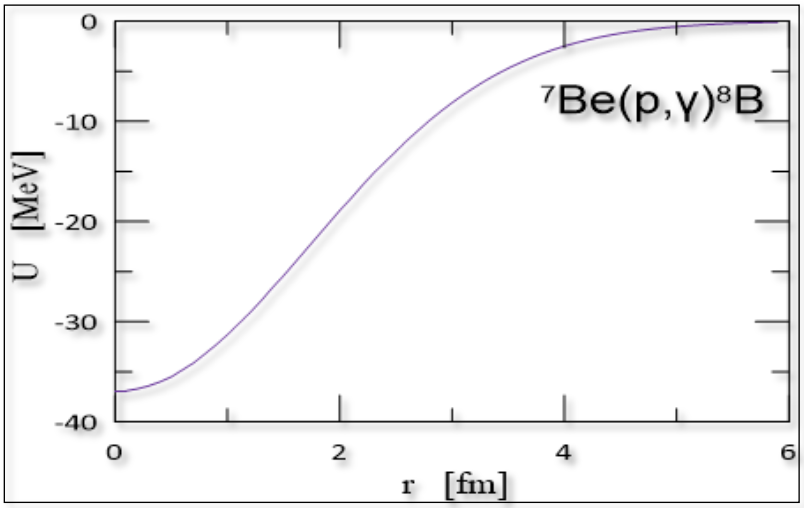

Figure 9. The WS model's representation of the potential of the ^{7}Be(p,γ)^{8}B reaction as a function of the radius

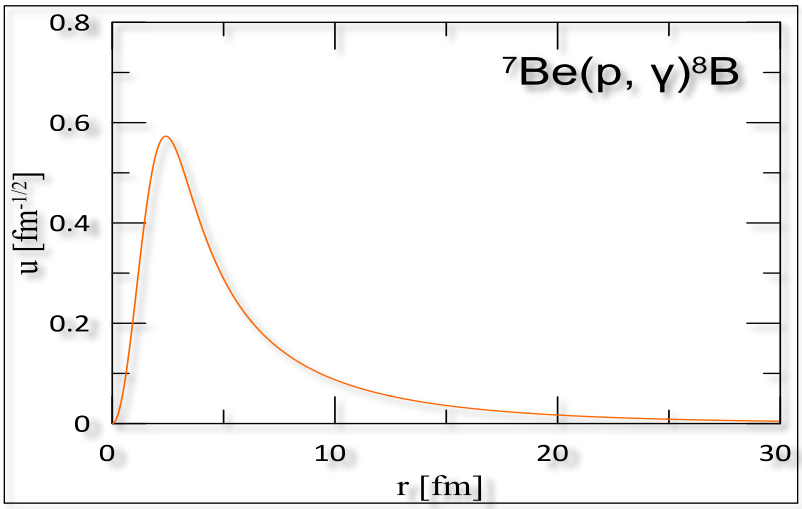

Figure 10. Normalized radial wave function u(r) of the 8B ground state formed in the 7Be(p, γ)8B reaction.

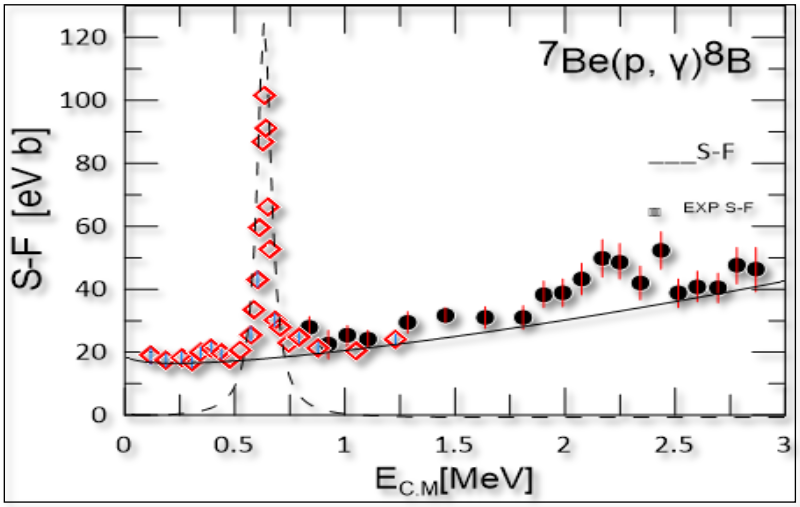

Figure 11. The S-F WS represents data derived from a theoretical model, while the S-F Exp represents results obtained from an experimental procedure [25] .

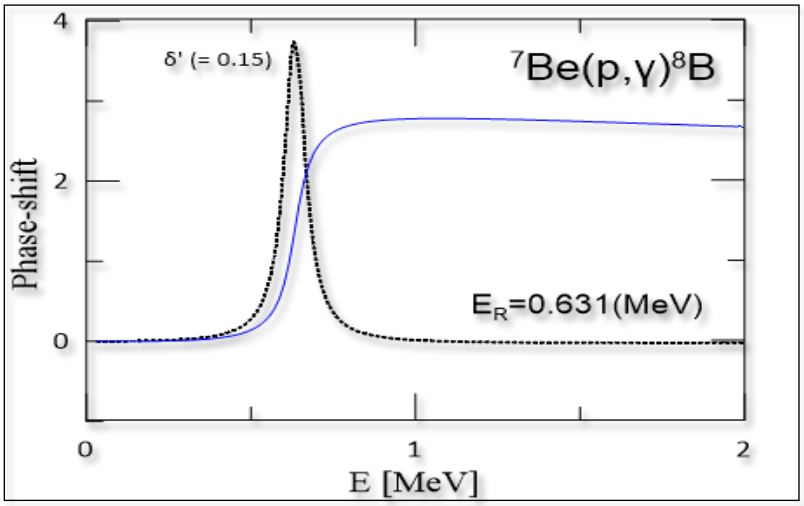

Figure 12. The ^{7}Be(p, γ)^{8}B system's phase shift (solid line) and its derivative (dashed line) are determined using the potential parameters resonance is detected at 0.631 MeV.

4.Discussion

4.1. ^{9}Be(p,γ)^{10}B

The ground state of ^{10}B, characterized by a spin-parity of $J_c=3^+$, is described by a proton in the $p_{3/2}$ orbital coupled to a ^{9}Be core with an intrinsic spin of $J_a=3/2^-$. For the direct capture DC process, the γ-ray transition is predominantly of E1 multipolarity, with the incoming waves primarily being s-type. The spectroscopic factor SF is assumed to be 1.0. The depth of potential for a continuum state Vc has been established at (−34.82 MeV) to maintain consistency with the results acquired using the R-matrix method [23] . **Figure 1** illustrates the radial dependence of the nuclear potential for the reaction, computed using the WS potential. The potential exhibits the typical profile of a mean-field nuclear potential a sharp increase from a deeply negative value at small radii, leveling off near the nuclear surface, and gradually approaching zero at larger distances. The depth of the potential well reaches approximately −28.5 MeV near the origin and slowly tends toward zero around r ≈ 6–7 fm, aligning with conventional parameterizations commonly applied to light nuclei. This potential effectively represents the strong, attractive nuclear force within the nucleus as the Coulomb repulsion near the surface, both of which are critical for accurately modeling bound and scattering states in radiative capture processes. **Figure 2** presents for the ground-state the radius wave function u(r) of the ^{9}Be(p,γ)^{10}B system. Plotted as this refers to a function whose value varies with the radial distance from the center of

the nucleus. As expected for a bound state in a finite potential well, the wave function exhibits a pronounced peak at $r \approx 2–2.5$ fm, indicating the most probable separation distance between the proton and the ^{9}Be core. Beyond this region, the amplitude decays exponentially. **Figure 3** theoretical predictions obtained using the WS potential model, illustrated by the solid red curve, are compared with experimental measurements represented by open circles. Within the energy range of approximately 0 to 1.6 MeV, the S-F remains relatively constant, indicating the dominance of non-resonant direct capture processes. This stability reflects the exponential suppression due to Coulomb repulsion in this low-energy region. As the energy increases from 0.5 MeV up to about 0.9 MeV, the S-F gradually rises, reaching a pronounced resonance peak near $E_{c.m}$=0.9 MeV with a maximum value of approximately 11.4 keV·b. This peak signifies the presence of a resonant state that enhances the reaction probability by improving Coulomb barrier penetrability and involving higher angular momentum partial waves. Following the resonance peak, the S-F decreases gradually with increasing energy, falling to about 0.7 keV·b at 1200 keV, while maintaining good agreement between theoretical predictions and experimental data throughout this energy range. Minor discrepancies observed in the 0.3–0.4 MeV region may be attributed to unresolved low-energy resonances or experimental uncertainties; however, these do not significantly affect the overall confidence in the (WS) model's ability to describe the reaction accurately. Overall, this analysis supports the use of the WS potential model for understanding low-energy proton capture mechanisms in the ^{9}Be(p,γ)^{10}B reaction, which is crucial for astrophysical applications, particularly in nuclear processes contributing to stellar energy generation.

4.2.^{7}Li(p, γ)^{8}Be

The present calculation pertains exclusively to the capture of the grounded state of ^{8}Be $J_c = 0^+$, which is defined as a proton with a charge of $p_{3/2}$ that is coupled to the ^{7}Li core, which has an intrinsic spin of $J_a = 3/2^-$. The incoming s and d waves and the E1 multipolarity dominate the gamma-ray transition [26]. To achieve the most accurate representation of the experiment data, the spectroscopy factor has been established at 1.0. The resonance at 0.4 MeV is generated by adjusting a potential depth to the continuum state, Vc = −77.72 MeV. The dashed line in the figure is the result obtained when Vc → 0 indicates the result without the effect of the 0.4 MeV resonance. **Figure 5** illustrates the radial dependence of the nuclear potential utilized in the of the ^{7}Li(p, γ)^{8}Be reaction, formulated using the WS potential. The potential well exhibits a characteristic depth of approximately −26.7 MeV. It extends spatially to reflect the finite range of nuclear forces, with the potential a radius of fm 6. The potential profile indicates a moderately diffuse nuclear surface, consistent with the chosen diffuseness parameter a_0=0.6. Such behavior of the potential well underpins the binding of the final-state system, in agreement with the bound state configuration of the ^{7}Li nucleus. **Figure 6** for the ground state of the ^{7}Li (p, γ)^{8}Be system, the radial wave function u(r) is presented as a function of the radial distance from the nuclear center. The wave function is normalized and exhibits a pronounced peak around r ≈(2-2.5) fm, corresponding to the most probable separation between the proton and the ^{7}Li core. **Figure 7** the S-F is also influenced by the resonance at 0.4 MeV, as evidenced by the experimental data from Ref [27] . The result of the capture at both the ground level and the first excited state is three times as large as the result for the ground state alone. It also examines the capture of the ground state. The S-F gradually increases at low energies, indicating the dominance of direct interactions between the particles and the nucleus. As the energy rises, the S-F reaches its resonance 0.4 MeV peak, where the particle's energy matches an internal nuclear energy level, significantly enhancing the reaction probability. After the resonance energy, the S-F gradually decreases due to the increasing dominance of Coulomb effects. **Figure 8** this analysis illustrates the energy dependence of the phase shift (solid blue line) and its derivative (dotted red line) for the ^{7}Li(p, γ)^{8}Be system, calculated using the WS potential model. The phase shift shows a sharp increase near the center-of-mass energy E_R=0.256 MeV, which clearly indicates a narrow resonance state within the compound nucleus ^{7}Li.

4.3. $^{7}Be(p, \gamma)^{8}B$

The ^{8}B is a $J_c = p_{3/2}$ coupled to the ^{7}Be core, with an intrinsic spin $J_a = 3/2^-$. In this instance, the values of a = 0.52 fm and V_{S0} = -9.8 MeV are derived from [25]. The incoming s and d waves and the E1 multipolarity dominate the gamma-ray transition. The spectroscopy factor was set to 1.0, the most effective reproducer. The S-F for the radiative capture in **Figure 11** the strong resonance effect at E=0.6 MeV, where increase in the S-F is observed, indicates the presence of a resonant state in the ^{8}B nucleus. This resonance significantly enhances the probability of interaction between the proton and ^{7}Be, leading to a notable increase in the reaction rate of $^{7}Be(p,\gamma)^{8}B$. This phenomenon can be explained by the strong coupling between the initial and final states through a resonant channel, resulting in a substantial amplification of the effective cross-section of the reaction. **Figure 12** shows a pronounced peak in the phase shift is observed at E=0.6 MeV, corresponding to a resonance energy of E_R=0.63 MeV. This indicates the presence of a resonant state, where the phase shift increases sharply, reflecting a significant enhancement in the interaction at this energy.

5. Conclusion

In this study, we have theoretically investigated the radiative proton capture reactions $^{9}Be(p, \gamma)^{10}B$, $^{7}Li(p, \gamma)^{8}Be$, and $^{7}Be(p, \gamma)^{8}B$ using a direct capture model with WS potentials. These reactions are important for stellar nucleosynthesis, particularly in stars undergoing hydrogen and helium burning processes. For the $^{9}Be(p, \gamma)^{10}B$ reaction, the calculated astrophysical S-F successfully match the experimental data across the energy range 0.1–1.6 MeV, with a maximum deviation of less than 7% and an RMS deviation of 0.08 keV·b. The model accurately reproduces the resonance at E_{cm}=0.9 MeV, with phase shift analysis confirming the narrow resonance behavior. For the $^{7}Li(p, \gamma)^{8}Be$ reaction, the theoretical S-F agrees with experimental results within 8% below 0.5 MeV, and it reproduces the narrow resonance near E_{cm}=0.4 MeV. The sensitivity analysis reveals that variations in the potential depth affect the S-F by approximately 10–15%, with the use of a spectroscopic factor SF = 1.0 improving the match for the resonance region. For the $^{7}Be(p, \gamma)^{8}B$ reaction, the model reproduces both the non-resonant behavior and the narrow resonance at E_{cm}=0.63 MeV, which corresponds to the $J\pi=1^+$ state in ^{8}B. The calculated S-F deviate by less than 9% from the experimental data, with an RMS deviation of 0.05 keV·b. Phase shift analysis independently confirms the position and presence of this resonance. The accurate modeling of this reaction is significant for understanding ^{8}B synthesis in stars and its impact on astrophysical processes.

Acknowledgment

We sincerely thank Prof. Dr. C.A. Bertulani, from National Superconducting Cyclotron Laboratory, Michigan State University, East Lansing, USA

Conflict of Interest

This article does not contain any conflicts of interest.

Funding

The article was done depending on self-fund and no establishments supplied us.

Ethical Clearance

The work and calculations were accomplished using the shell model code RADCAP (2003) developed by Prof. Dr. C.A. Bertulani from Michigan State University.

References

1. Brune CR, Davids B. Radiative capture reactions in astrophysics. Annu Rev Nucl Part Sci. 2015;65(1):87–112.https://doi.org/10.1146/annurev-nucl-102014-022027
2. Burbidge EM, Burbidge GR, Fowler WA, Hoyle F. Synthesis of the elements in stars. Rev Mod Phys. 1957;29:547–650.https://doi.org/10.1103/RevModPhys.29.547
3. Denissenkov PA, Herwig F, Perdikakis G, Schatz H. The impact of (n,γ) reaction rate uncertainties of unstable isotopes on the i-process nucleosynthesis of the elements from Ba to W. Mon Not R Astron Soc. 2021;503(3):3913–3925.https://doi.org/10.1093/mnras/stab3504
4. Wiescher M. The history and impact of the CNO cycles in nuclear astrophysics. Phys Perspect. 2018;20(1):124–158.https://doi.org/10.1007/s00016-018-0216-0
5. Bahcall JN, Ulrich RK. Solar models, neutrino experiments, and helioseismology. Rev Mod Phys. 1988;60(2):297–372.https://doi.org/10.1103/RevModPhys.60.297
6. Simon A, Koros J, Olivas-Gomez O, Kelmar R, Churchman E, Clark AM, Harris C, Henderson SL, Kelly SE, Millican P, Palmisano-Kyle A, Reingold CS, Robertson D, Stech E, Spyrou A, Tan WP. Proton capture on ^{90}Zr revisited. Eur Phys J A. 2025;61(3):57. https://doi.org/10.1140/epja/s10050-025-01521-9
7. Kravvaris K, Navrátil P, Quaglioni S, Hebborn C, Hupin G. Ab initio informed evaluation of the radiative capture of protons on ^{7}Be. Phys Lett B. 2023;845:138156. https://doi.org/10.1016/j.physletb.2023.138156
8. Dalvand M, Khalili H. Electromagnetic transition strengths on the S-factor for radiative capture proton by ^{17}O. Chinese Phys *C*. 2014;38(8) 08410110. https://doi.org/1088/1674-1137/38/8/084101
9. Prantzos N. CNO cycle. In: Encyclopedia of Astrobiology. Springer; 2023. p. 608.
10. Iliadis C, Longland R, Champagne AE, Coc A, Fitzgerald R. Charged-particle thermonuclear reaction rates: II. Nucl Phys A. 2010;841:31–250.https://doi.org/10.1016/j.nuclphysa.2010.04.009
11. Irgaziev BF, Nabi JU, Kabir A. Radiative capture of proton by C-12 at low energy. Astro phys Space Sci. 2018;363:148.https://doi.org/10.1007/s10509-018-3365-0
12. Kabir A, Nabi JU, Sagheer S, Rashid L. Radiative capture of proton by ^{9}Be(p,γ)^{10}B at low energy. Commun Theor Phys. 2022;74:025301.https://doi.org/10.1088/1572-9494/ac47ae
13. Kharab R. Dependence of B(E2) and B(M1) transition strengths on energy and spin of excited states of ^{18}F. Mod Phys Lett A. 2018;33:1850188.https://doi.org/10.1142/S0217732318501884
14. Radhi RA, Alzubadi AA. Study the nuclear form factors of low-lying excited states in ^{7}Li nucleus. Few-Body Syst. 2019;60:57.https://doi.org/10.1007/s00601-019-1524-x
15. Descouvemont P, Baye D. The R-matrix theory. Rep Prog Phys. 2010;73:036301. https://doi.org/10.1088/0034-4885/73/3/036301
16. Kabir A, Nabi JU. Re-examination of proton capture ^{13}N(p,γ)^{14}O in stellar matter. Phys Scr. 2020;96:015305.https://doi.org/10.1088/1402-4896/aba3d6
17. Radhi RA, Alzubadi AA, Ali AH. Calculations of the quadrupole moments for some nitrogen isotopes. Iraqi J Sci. 2017:878–883.
18. Khalili H, Mohammadzadeh M. The astrophysical S-factor of proton radiative capture on triton. New Astron. 2021;86:101572.https://doi.org/10.1016/j.newast.2021.101572
19. Mondal SH, Khan MA. Study of fusion cross-section and astrophysical S-factor for p+^{15}N and α+^{12}C. Int J Mod Phys E. 2022;31:2250045.https://doi.org/10.1142/S0218301322500456
20. Ali LT, Selman AA. Non-resonant reaction rates of ^{13}C(α,n)^{16}O and ^{22}Ne(α,n)^{25}Mg. Iraqi J Sci. 2021.
21. Iliadis C, Wiescher M. Spectroscopic factors from direct proton capture. Phys Rev C. 2004;69:064305.https://doi.org/10.1103/PhysRevC.69.064305
22. Huang JT, Bertulani CA, Guimarães V. Radiative capture of nucleons at astrophysical energies. At Data Nucl Data Tables. 2010;96:824–847.https://doi.org/10.1016/j.adt.2010.06.001
23. Sattarov A, Mukhamedzhanov AM, Azhari A, Gagliardi CA, Trache L, Tribble RE. Astrophysical S factor for ^{9}Be(p,γ)^{10}B. Phys Rev C. 1999;60:034611. https://doi.org/10.1103/PhysRevC.60.034611
24. Zahnow D, Angulo C, Rolfs C, Schmidt S, Schulte WH, Somorjai E. The S(E) factor of ^{7}Li(p,γ)^{8}Be. Z Phys A. 1995;351:229–236.https://doi.org/10.1007/BF01293195
25. Junghans AR, Mohrmann EC, Snover KA, Steiger TD, Adelberger EG, Casandjian JM, Swanson HE, Buchmann L, Park SH, Zyuzin A, Laird AM. Precise measurement of the ^{7}Be(p,γ)^{8}B S factor. Phys Rev C. 2003;68:065803.https://doi.org/10.1103/PhysRevC.68.065803

26. Dubovichenko SB, Dzhazairov-Kakhramanov AV, Burkova NA. Reaction rate of the ^{7}Li(p,γ)^{8}Be. Nucl Phys A. 2021;1015:122312.https://doi.org/10.1016/j.nuclphysa.2021.122312
27. Inoue A, Tamii A, Chan P, Hayakawa S, Kobayashi N, Maeda Y, Nonaka K, Shima T, Shimizu H, Tran DT, Wang X. Contribution of the ^{7}Be(d,p) reaction to the ^{7}Li problem. J Phys Conf Ser. 2020;1643:012049.https://doi.org/10.1088/1742-6596/1643/1/012049